Chapter 8
Wall-layer models for LES of separated flows

G. Valter Diurno, Elias Balaras, Ugo Piomelli

Department of Mechanical Engineering, University of Maryland, College Park, MD, USA

Abstract In order to extend large-eddy simulation (LES) to practical engineering and aeronautical applications, wall-layer model are required. In the present study recent developments in this field are presented. A new version of the two-layer model (TLM) is proposed and tested in a separated flow. The TLM methodology is based on a zonal approach, in which the computational domain is divided in an outer-flow region, where the filtered Navier-Stokes equation are solved and an inner-layer, near the solid walls. In this layer a simplified set of equations is solved and the effect of all turbulent structures is modeled. A limit of the TLM formulation, as used so far, is that an algebraic turbulence model is used to parameterize the effect of turbulence in the inner-layer. Although, the results in equilibrium flows were very satisfactory, some loss of accuracy is expected in separated flows. To account for the more complex physics in this type of flows a more advanced turbulent model, namely the Spalart-Allmaras model [*Rech. Aérospatiale* **1**, 5–21, (1994)] is introduced. The results obtained for the backward-facing-step flow agree well with the reference data.

8.1 Introduction

Despite the impressive advances of Computational Fluid Dynamics in the past thirty years, turbulence remains a challenging problem. The most common numerical approach to deal with turbulent flows is to devise a model able to take into account the overall effect of turbulence on the mean flow quantities. This is the basic assumption behind the Reynolds-Averaged Navier-Stokes (RANS) approach. The RANS equations are derived from the Navier Stokes equations by using a time-average or ensemble-average operator. This procedure introduces additional unknowns that have to be modeled in order to close the system of equations. The empiricism and the assumptions that underlie the construction of such models are a major obstacle in the establishment of the RANS approach as a reliable predictive tool. This is directly linked to the fact that in the RANS methodology one attempts to calculate a turbulent flow field without actually resolving the turbulent eddies, but using a model which is linked to the mean flow only.

A different approach, which does not suffer from the above drawbacks since all scales of motion are resolved, is the Direct Numerical Simulation (DNS). In this case the Navier-Stokes equations are solved without introducing any kind of modeling. The amount of data that the simulation generates can be compared to an experiment with millions of unobtrusive probes. The scientific community agrees that the value of a DNS and an experiment are comparable, and that DNS is a valuable tool to perform "experiments" without the limitations of the experimental apparatus. The DNS approach, however, is limited to the computation of fairly simple flows at very low Reynolds numbers because of the large computational resources that it requires.

In order to have an estimate of the cost of a DNS, we observe that all the scales of motion including the dissipative ones must be resolved, and the computational domain should be sufficiently large to contain the largest structures present in the flow field. In addition, the time-step must be smaller than the smallest time-scale. The ratio between the largest (L = the size of the computational domain) and smallest (η = the Kolmogorov scale) scales can be estimated to be $L/\eta \sim Re^{3/4}$. Thus, the number of points required by a DNS in three dimensions is $N \sim Re^{9/4}$. The same proportionality, $Re^{1/4}$, holds for the ratio between the integral time-scale to the Kolmogorov time-scale. Thus we have a cost proportional to Re^3, if we assume that the CPU time required by the numerical algorithm is proportional to the number of grid points N. Since Reynolds numbers of the order one million or more are quite common in engineering applications, DNS remains still impracticable, with the present computer power, for this kind of flows.

An alternative approach is the Large-Eddy Simulation (LES), which can deal with considerably higher Reynolds numbers than DNS, while keeping many of its advantages. In LES only the large, energy-carrying structures are computed, while the small scales are modeled. With this methodology the large scales that are flow-specific and strongly depend on the boundary conditions are resolved as in the DNS approach. The small scales, which are believed to be approximately homogeneous and isotropic, can be parametrized by simple eddy-viscosity models.

Over the past decades, LES has been used to simulate flows in simple geometries, similar to those studied by DNS, albeit at a higher Reynolds numbers. However, to deal with technologically relevant flows, a method should be flexible enough to be used on complex geometries at a reasonable cost. Only recently a significant effort to extend LES to more complex geometries has been started; however, the method is still too expensive at high Reynolds numbers because of the resolution requirements of the near-wall layer, which demand a number of points almost as large as in a DNS.

When a solid wall is present, in fact, the structures near the wall be-

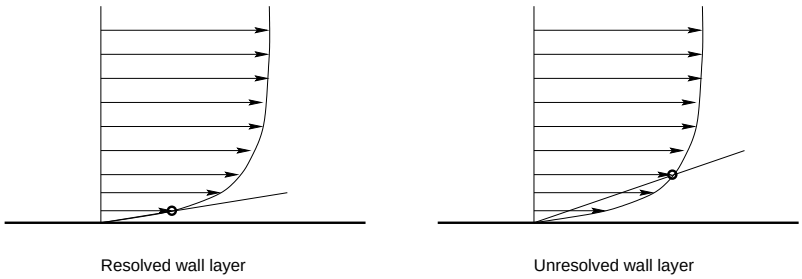

Figure 8.1: Evaluation of the wall stress.

come very small and the resolution requirements in terms of grid points become very strict. For example, in a boundary layer over a flat plate, streaks appear in the near-wall region. These elongated structures, that are responsible for much of momentum transfer, measure about 2000 wall units in the streamwise direction, 20 to 80 wall units in width and their distance in the spanwise direction is about 100 wall unit ["wall units" are defined as $X_i^+ = X_i u_\tau / \nu$ with $u_\tau = \sqrt{\tau_w/\rho}$, $\tau_w = \mu(\partial u/\partial z)_w$, μ being the viscosity and ρ the density]. In order to resolve the wall layer we need a domain that contains a sufficient sample of these structures and an adequate number of grid points. If the length of the domain is L_i for $i = 1, 2, 3$ and the spacing is ΔX_i, the number of points is $N_i = L_i/\Delta X_i$. If we require ΔX_i^+ constant, we can easily obtain that $N \simeq Re^{2.6}$ (Chapman 1974). In the outer flow, the structures are larger and they scale with the dimension of the boundary layer, and a similar estimate gives $N \simeq Re^{0.4}$ (Chapman 1974). Thus, when the wall layer is resolved, LES is also limited to moderate Reynolds numbers.

To circumvent the high cost incurred when the near-wall layer is resolved, one can bypass it altogether, and model its effects in a statistical sense. Modeling the wall layer makes the cost of a calculation proportional to $Re^{0.4}$. However, this process introduces further empiricism; the challenge is to keep it at a reasonable level. Consider the sketch in Fig. 8.1; when the wall layer is resolved, no-slip boundary conditions can be used for the velocity field, and the wall stress can be obtained by simple differentiation. On the other hand, when the wall layer is not resolved, the use of no-slip conditions results in severe underestimation of the wall shear stress. Thus, the main objective of a wall-layer model should be to give a reasonable estimate of the local/instantaneous wall shear stress, that can be used as a Neumann boundary condition for the velocity field.

Most of the proposed "wall-layer models", or "approximate boundary conditions", assume that the dynamics of the wall-layer are universal and

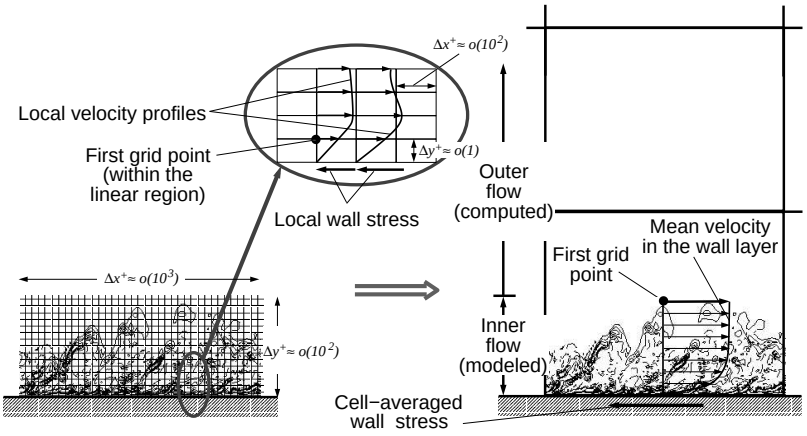

Figure 8.2: Sketch of the two-layer-model concept.

that some generalized law-of-the-wall exists. Deardorff (1969) forced the existence of a logarithmic layer, and assumed that turbulence is isotropic in the near-wall layer by imposing conditions for the second derivatives of the streamwise and spanwise velocity components. Schumann (1974) correlated the wall stresses and velocity in the core of the flow by

$$\tau_{xz} = \frac{<\tau_w>}{<\overline{u}(x,y,z_2)>}\overline{u}(x,y,z_2), \tag{8.1}$$

$$\tau_{yz} = \frac{1}{Re_\tau}\frac{<\overline{v}(x,y,z_2)>}{\Delta z/2}. \tag{8.2}$$

In these equations, x, y, z are the streamwise, spanwise and normal direction respectively, u, v, w are the corresponding velocities components and z_2 indicates the coordinate of the first grid point off the wall in the wall-normal direction. The brackets indicate average over homogeneous directions. The mean wall stress, $<\tau_w>$ in case of channel flows can be estimated from the pressure gradient, or can be computed by imposing the logarithmic law. Piomelli *et al.* (1989) proposed a modification to this model that takes into account the structure and orientation of the elongated structures present in the near-wall region.

A different approach has been proposed by Balaras and Benocci (1994) and Balaras *et al.* (1996), in which the filtered Navier-Stokes equations are solved in the core of the flow, while in the wall-layer a simplified set of equations is solved and the effect of all scales of motions is modeled. Consider the sketch in the Figure 8.2. If the cell near the wall is much larger than the typical near-wall eddy size, it will contain a large number of such eddies. Because of the large grid size, the time-step will be larger

than the typical life-cycle of those eddies so that, in one time-step, a large number of small eddies are generated and destroyed within that cell. In this "Two-Layer Model" (TLM), instead of resolving all structures, only their overall effect is taken into account through the cell-averaged wall stress, which is the output of the inner-layer calculation.

The basic assumption behind this technique is that the interaction between the near-wall region and the outer region is weak. Support for this assumption, at least for equilibrium flows, can be found in Brooke and Hanratty (1993). By analysis of DNS databases of a turbulent channel flow they found that, near the wall, the structures regenerate themselves and no interaction with the outer flow structures was detected.

The TLM uses the boundary layer equations in the inner layer:

$$\frac{\partial \overline{u}_i}{\partial t} + \frac{\partial}{\partial x_1}(\bar{u}_n \bar{u}_i) = -\frac{\partial \overline{p}}{\partial x_i} + \frac{\partial}{\partial x_n}\left[(\nu + \nu_t)\frac{\partial \bar{u}_i}{\partial x_n}\right] \tag{8.3}$$

where n indicates the normal direction and i spans 1,2 or 1,3 depending on whether the wall plane is the $x-y$ or $x-z$ plane. The unknown normal velocity u_n is computed by imposing mass conservation in the inner layer.

In Balaras and Benocci (1994) and Balaras *et al.* (1996) an algebraic eddy viscosity model was used to parameterize all scales of motion in the wall layer:

$$\nu_t = (\kappa z)^2 D(z) \left|\overline{S}\right| \tag{8.4}$$

where κ is the von Kármán constant, z is the distance from the wall, $\left|\overline{S}\right|$ is the magnitude of the strain rate tensor, and $D(z)$ is a damping function that assures the correct behavior of ν_t at the wall:

$$D(z) = 1 - \exp\left[-\left(z^+/A^+\right)^3\right] \tag{8.5}$$

where $A^+ = 25$. Other, more complex models, can be used in the near-wall layer to extend this approach to non-equilibrium flows (see below).

While the TLM has given good results in equilibrium or quasi-equilibrium flows (Balaras *et al.* 1996), its application to more complex geometries are limited. Cabot (1995) and Cabot and Moin (1999) computed a backward-facing step flow at high Reynolds number. More recently, Wang (1999) used the TLM for a trailing-edge aero-acoustics calculation.

The purpose of this article is to evaluate the accuracy of the TLM approach in a separated flow, the flow over a backward-facing step, using a more advanced inner-layer turbulence model. In configurations that include separation, pressure gradients or mean-flow three-dimensionality, one cannot expect the simple mixing-length model (8.4) to give accurate results. On the other hand, one should not increase tremendously the

complexity (and cost) of the calculation. We have chosen the Spalart-Allmaras (1994) one-equation eddy-viscosity model, that has been shown to give accurate prediction of the flow in attached boundary layers, and is recently being proposed as a wall-layer model as well within the Detached Eddy Simulation framework (Nikitin *et al.* 2000).

In the following, the governing equations and the formulation of the inner-layer model will be presented. Then, in Section 8.3, some results will be presented and discussed. Finally, some conclusions will be drawn.

8.2 Formulation

8.2.1 Numerical method and subgrid-scale model

The governing equations for incompressible LES are the filtered Navier-Stokes equations

$$\frac{\partial \overline{u}_i}{\partial t} + \frac{\partial}{\partial x_j}(\overline{u}_i \overline{u}_j) = -\frac{\partial \overline{p}}{\partial x_i} - \frac{\partial \tau_{ij}}{\partial x_j} + \frac{1}{Re}\frac{\partial^2 \overline{u}_i}{\partial x_j \partial x_j}, \tag{8.6}$$

$$\frac{\partial \overline{u}_i}{\partial x_i} = 0, \tag{8.7}$$

where $\overline{u}_i$ are the large scale velocity components, $\overline{p}$ is the pressure and Re is the Reynolds number. The previous equations can be obtained from the Navier-Stokes equations by the application of a filtering operation that separates the large resolved scales from the small ones. The coupling between the large and the small scales appears in the form of a subgrid-scale stress tensor $\tau_{ij} = \overline{u_i u_j} - \overline{u}_i \overline{u}_j$, that needs to be modeled. In the present work, the localized dynamic model (Piomelli and Liu 1995) is used to parameterize the SGS stresses.

Equations (8.6) and (8.7) are advanced in time using an explicit Adams-Bashforth fractional-step method. That involves the solution a Poisson-like equation that links pressure and velocity fields at each time step. A direct-solver was used for the solution of this equation. All derivatives were approximated with second-order central finite-differences on a staggered grid. Details on the numerical method and the treatment of near-wall boundaries can be found in Balaras *et al.* (1995)

8.2.2 The Two-Layer Model

A limit in the TLM formulation as described above is that an algebraic turbulence model is used to parameterize the effect of turbulence in the inner, near-wall layer. Cabot (1995) used the Johnson-King (1989) model that is said to be a *half-equation* model, but in practice is only a more

advanced algebraic model. The use of the TLM in high Reynolds number non-equilibrium flows requires that a more advanced turbulence model should be introduced. We have chosen the one-equation model of Spalart-Allmaras (1994) for its simplicity and quality of results, even compared with more complex multi-equation turbulence models. The equation solved is a transport equation for the quantity $\tilde{\nu}$, which is related to the eddy viscosity ν_t:

$$\frac{D\tilde{\nu}}{Dt} = c_{b1}\tilde{S}\tilde{\nu} + \frac{1}{\sigma}\left\{\nabla\cdot[(\nu+\tilde{\nu})\nabla\tilde{\nu}] + c_{b2}(\nabla\tilde{\nu})^2\right\} - c_{w1}f_w\left[\frac{\tilde{\nu}}{d}\right]^2 \tag{8.8}$$

in which the material derivative on the LHS contains the unsteady and advective terms. The first group in the RHS is the production term, the second is a diffusion term, and finally there is a destruction term. The other quantities in (8.8) are given by:

$$\begin{aligned}
\widetilde{S} &= S + \frac{\tilde{\nu}}{k^2d^2}f_{\nu 2},\\
f_{\nu 2} &= 1 - \frac{\chi}{1+\chi f_{\nu 1}}\\
\nu_t &= \tilde{\nu}f_{\nu 1},\\
f_{\nu 1} &= \frac{\chi^3}{\chi^3 + c_{\nu 1}^3}\\
\chi &\equiv \frac{\tilde{\nu}}{\nu}\\
f_w &= g\left[\frac{1+c_{w3}^6}{g^6+c_{w3}^6}\right],\\
g &= r + c_{w2}(r^6 - r)\\
r &\equiv \frac{\tilde{\nu}}{\tilde{S}k^2d^2},
\end{aligned}$$

and the constants are:

$$\begin{aligned}
c_{b1} &= 0.1355,\\
\sigma &= 2/3,\\
c_{b2} &= 0.622,\\
\kappa &= 0.41,\\
c_{w1} &= c_{b1}/k^2 + (1+c_{b2})/\sigma,\\
c_{w2} &= 0.3,\\
c_{\nu 1} &= 7.1.
\end{aligned}$$

The model constants have been evaluated using several building block flows (Spalart and Allmaras 1994). The use of $\tilde{\nu}$ instead of the eddy viscosity is justified by the fact that, unlike ν_t, the new variable behaves linearly near the wall and does not require the use of damping functions that are so widespread in many turbulence models.

Production, destruction and also the diffusion terms are all non-linear and in particular the latter can be cast in many different forms. The equation has been discretized using central differences and advanced in time implicitly. At the solid wall $\tilde{\nu}$ is set to zero, while at the interface with the outer flow, a suitable value for $\tilde{\nu}$ must be specified. This is a complication compared to the algebraic model, that did not require such a condition. However, this boundary condition introduces a stronger coupling between the inner-layer and the outer-flow. Two possibilities have been considered to find a reasonable value for ν_t at the interface: one can impose the matching of the total stress:

$$-(\overline{u}_i\overline{u}_j) + 2(\nu + \nu_t^o)\overline{S}_{ij}^o = -(U_iU_j) + 2(\nu + \nu_t^i)\overline{S}_{ij}^i \tag{8.9}$$

where on the left hand side we have quantities computed using the resolved LES variables, and on the right hand side, the same quantities are computed using the inner-layer variables ($\overline{S}_{ij}$ indicates the strain rate tensor and the exponents o and i indicate outer-flow and inner-layer variables). If the velocity field is continuous at the interface (C^1), this expression reduces to:

$$\nu_t^i = \nu_t^o \tag{8.10}$$

Since the velocity boundary conditions are forcing the velocity field at the interface to be C^0, however, the above relation is correct only in an approximate sense. The use of (8.9), however, gave rise to numerical instabilities, while (8.10) was found to be better behaved and result in total stresses that where continuous at least in a statistical sense.

8.3 Results

The new treatment of the wall layer was first tested in simple attached flows (plane channel, flat-plate boundary layer), in which it gave results in good agreement with the DNS, resolved LES and experimental data. It was then applied in a more challenging case, the flow over a backward-facing step (Fig. 8.3). Separation takes place due to the abrupt change in the geometry, and much of the flow is dominated by an inviscid shear layer departing from the corner point. The flow reattaches several step-heights downstream of the corner, depending on the Reynolds number, and recovers further downstream, approaching an equilibrium boundary

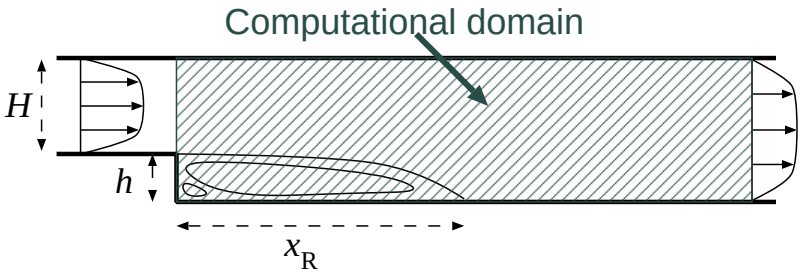

Figure 8.3: Backward-facing step configuration.

Table 8.1: Computational parameters.

Case	Re_h	Outer grid	Embedded grid
1	5100	140×32×48	140×32×21
2	28000	160×32×80	160×32×31

layer.

Two cases were studied, for which DNS, experimental or resolved LES data are available. For the first, low-Reynolds number case, the inflow is a fully developed boundary layer with Reynolds number $Re_{\delta^*} = 770$ based on free-stream velocity, U_o, and displacement thickness, δ^*, at the domain inlet. DNS data by Le and Moin (1994) are available for this case. The computational domain is a box whose dimensions are $25h \times 4h \times 6h$ in the streamwise, spanwise and normal directions respectively ($h = 6.67\delta^*$ is the step height), which was discretized using a Cartesian grid. The grid points for the outer LES computation were distributed in such a way that the inviscid shear layer departing from the step edge was properly resolved. Care was also taken in allocating a minimum of 10×10 grid points at the location of the secondary bubble, near the step corner. To fulfill these requirements the grid was uniform in the spanwise (y) and the normal directions (z), and stretched in the streamwise direction (x). For the inner-layer calculation the same number of grid points as in the outer computation was used in the streamwise and spanwise directions; 21 equally spaced points were used in the normal direction. The inner layer grid could be much coarser in the streamwise and spanwise directions, without loss of accuracy; the cost of inner layer calculation, however, is only a fraction of that of the outer LES, and thus the present choice does not increase dramatically the overall cost. All computational

parameters for both cases are given in Table 1.1

A similar grid arrangement was adopted for the high Reynolds number case ($Re_h = 28000$). In this case, however, the inflow is formed by two boundary layers separated by an inviscid core at a much higher Reynolds number, $Re_{\delta^*} = 4200$. The computational domain size is $23h \times 2h \times 5h$ in the streamwise, spanwise and normal directions respectively. As can be seen in Table 1.1, a larger number of points in the non-homogeneous directions is used in this case in order to resolve the inviscid shear layer properly. Resolved LES (Akselvoll and Moin 1995) and experimental (Adams *et al.* 1984) data is available for this case.

Figures 8.4 and 8.5 show the mean streamlines and the velocity vectors for the low and high Reynolds-number cases respectively. The velocity field predicted by the TLM is also added in the figure; the thin horizontal line denotes the interface between the two zones. The main features of the flow are captured correctly. The velocity fields resulting from the outer LES, and inner TLM computations exhibit a fair degree of continuity at the interface, indicating that the present coupling through the velocity and turbulent viscosity boundary conditions is sufficient.

The reattachment point is predicted very accurately in both cases. For Case 1 (Figure 8.4c) it is $6.5h$, which agrees well with the value of $6.6h$ reported in the DNS of Le and Moin (1994). For Case 2 (Figure 8.5c) the reattachment point is $6.6h$, also in good agreement with the resolved LES of Akselvoll and Moin (1995). In general, in all calculations performed in the framework of this study, the type of turbulence model that was used in the TLM (algebraic or Spalart-Allmaras model) was found to have a small effect on the location of the reattachment point; its location was mainly influenced by the numerical resolution near the edge of the step, which is related to proper development of the inviscid instability. In both cases the secondary bubble that is present at the step corner was also captured accurately (Figs. 8.4b and 8.5b). For the low-Reynolds number case it has similar size (approximately $1/2h$) and shape as in the one reported in the DNS. For the high Reynolds number, however, its structure appears to be significantly different.

It should also be pointed out that even in the separated flow region the flow in the inner layer is attached (Figs. 8.4b,c and 8.5b,c), which justifies somewhat the use of the boundary-layer equations. However, near the reattachment point the flow at the edge of the inner layer is subjected to a strong acceleration (Figs. 8.4c and 8.5c); thus, equilibrium models such as those based on the logarithmic law (such as the algebraic mixing length model itself) cannot be expected to be accurate. This can be seen more clearly in Fig. 8.6, in which the distribution of the skin friction coefficient along the bottom wall is shown for Cases 1 and 2 respectively.

In the low-Reynolds number case the flow is too slow in the recirculating region when the algebraic model is used. The opposite trend can

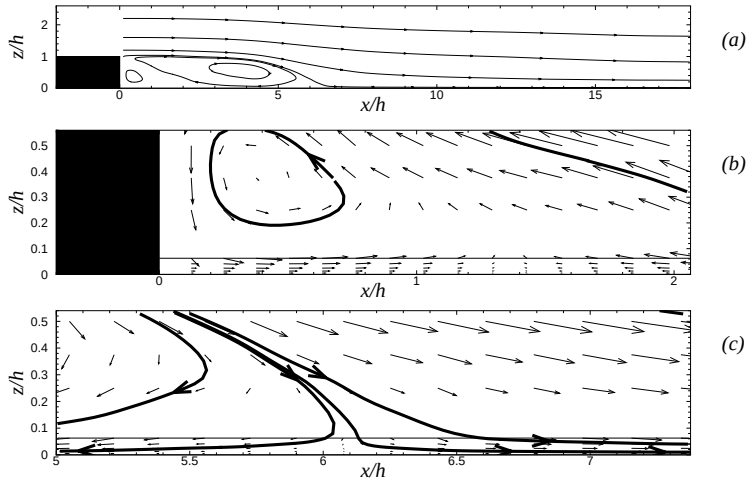

Figure 8.4: Backward-facing step, low Reynolds number. Mean streamlines and velocity vectors. (a) Global view; (b) corner region; (c) reattachment region. The thin horizontal line indicates the interface between inner and outer layer.

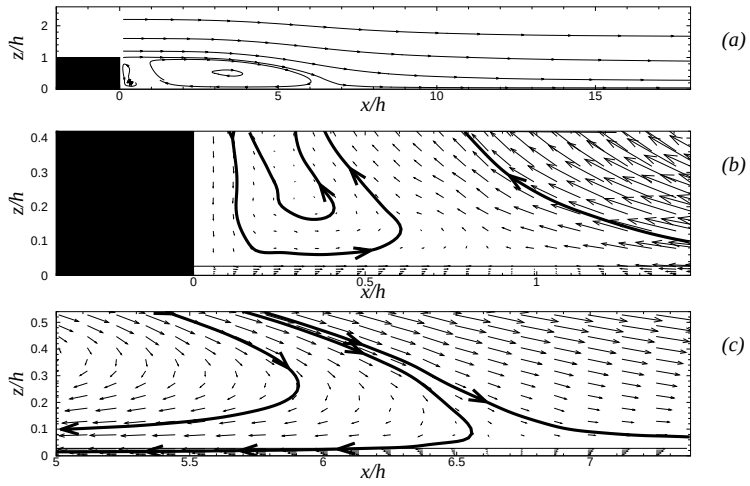

Figure 8.5: Backward-facing step, high Reynolds number. Mean streamlines and velocity vectors. (a) Global view; (b) corner region; (c) reattachment region. The thin horizontal line indicates the interface between inner and outer layer.

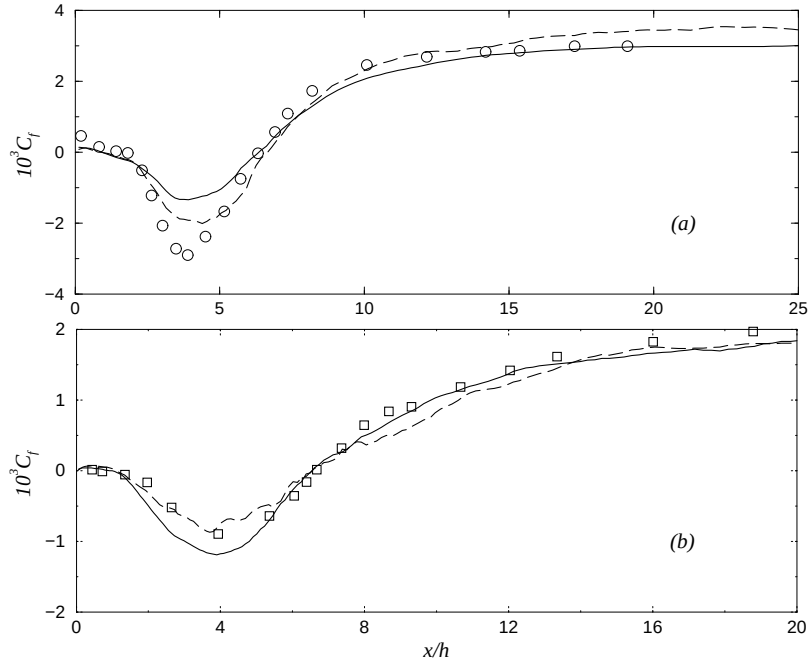

Figure 8.6: Backward-facing step, Skin-friction coefficient. ◦ DNS data (Le and Moin 1994), □ Experimental data (Adams *et al.* 1984), —— TLM-Algebraic, — — — TLM-SA. (a) Low Reynolds number; (b) high Reynolds number.

been seen in the high-Reynolds number case, where the flow is a little faster in the recirculating region. The later result is in agreement with the findings of Cabot (1995), who calculated the flow over a backward facing step using the TLM coupled with an algebraic eddy viscosity model. In a more resent paper Cabot and Moin (1999) reported improved results for this flow when κ in equation (8.4) was computed "dynamically". A series of calculations (not reported here) which were carried out in in the framework of this study, with different values of κ, or different expressions for the damping function $D(z)$ in equation (8.4) showed a great sensitivity of the results to these parameters. The TLM coupled with the Spalart-Allmaras turbulent model, on the other hand, appears to be more accurate and robust. The predicted skin-friction coefficient for both Reynolds numbers is in good agreement with the reference data (Fig. 8.6).

The mean velocity profiles for the low-Reynolds number case are shown in Fig. 8.7a at various streamwise locations. The agreement with the DNS data by Le and Moin (1994) is very good. The error introduced by the wall model is limited to the first grid point off the wall. The differences between the results obtained with the algebraic and the Spalart-Allmaras turbulence model are very small for the mean flow quantities. The larger differences observed in the skin friction coefficient above are not reflected here, since the streamwise freestream velocity is used to scale the velocity field. A similar trend can be seen in the streamwise velocity fluctuations and Reynolds shear stress shown in Figs. 8.7b and 8.7c, which also agree well with the reference DNS data. Similar considerations can be drawn from the corresponding quantities shown in Fig. 8.8 for the high-Reynolds number case.

In an attempt to examine the coupling between the inner and outer layer and the reaction of the TLM computation to the perturbations imposed from the outer flow, several instantaneous velocity fields were examined. In the bottom part of Figure 8.9 isolines of the predicted wall shear stress are shown. The thick lines are the instantaneous reattachment lines for the primary and secondary recirculation bubbles. The velocity vectors and streamlines for the cross sections marked on these lines can be seen on the top part of the figure. The velocity field at the interface appears to be continuous. The TLM computation is clearly driven by the outer LES calculation and reacts to the imposed perturbations. In Section BB for example in Figure 8.9, the inner-layer field adjusts to the strong "ejection" event coming from the outer flow. In general, in this and also other realizations examined the coupling between the two computations appears to be strong despite the approximations involved.

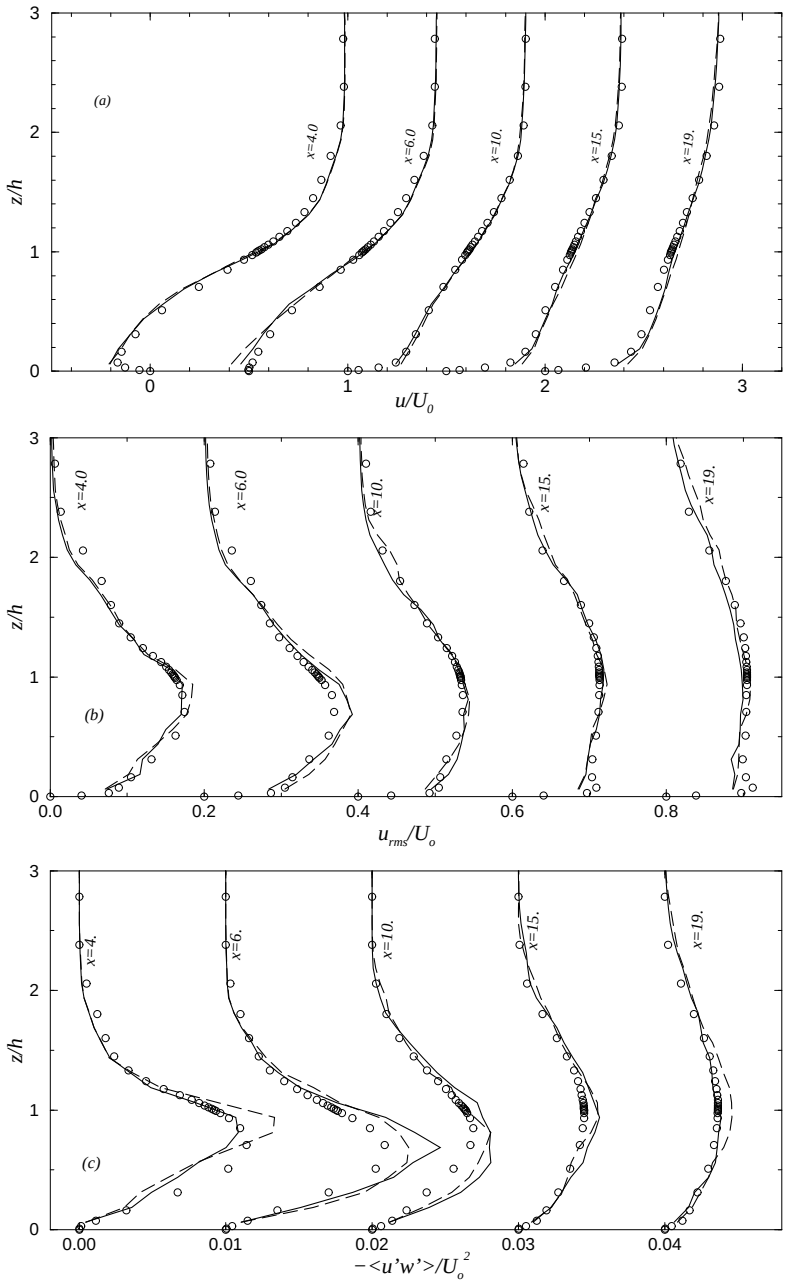

Figure 8.7: Backward-facing step, low Reynolds number. (a) Mean velocity; (b) streamwise turbulence intensity; (c) Reynolds shear stress. ◦ DNS data (Le and Moin 1994), —— TLM-Algebraic, — — — TLM-SA.

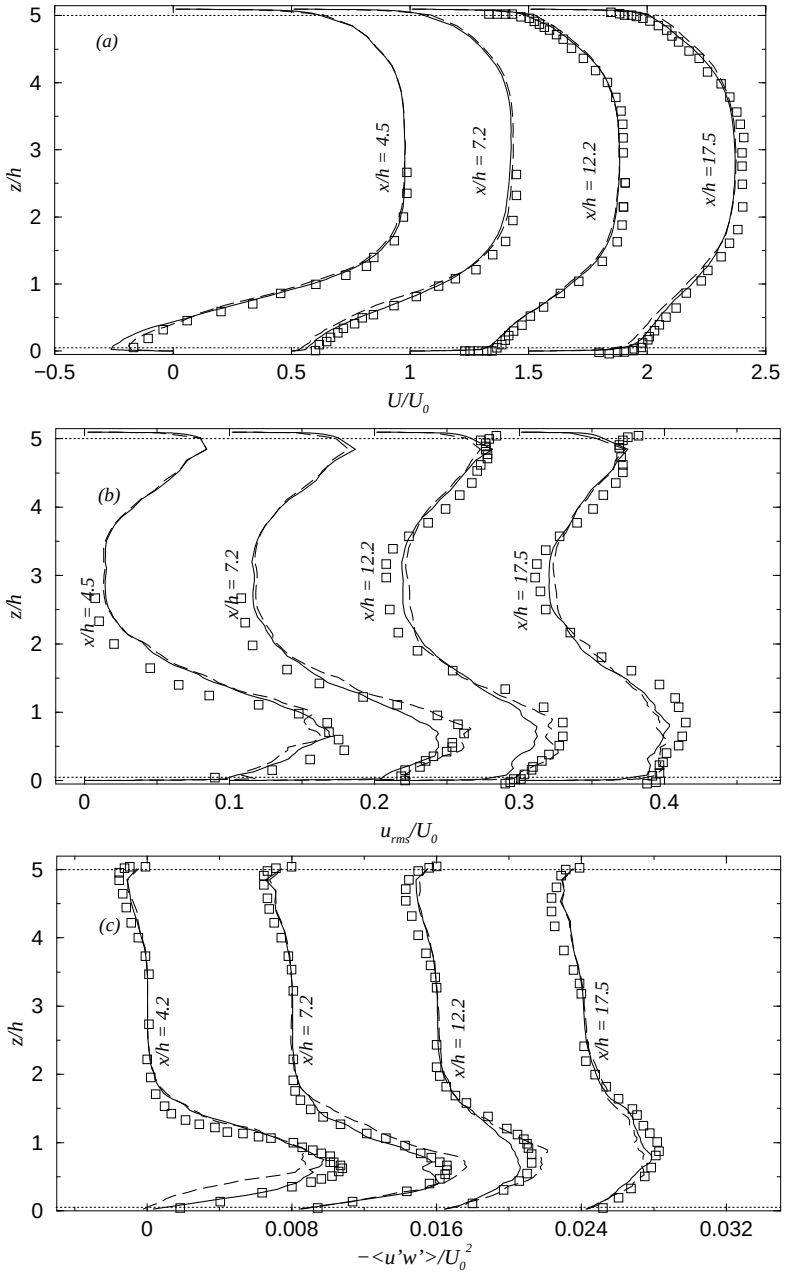

Figure 8.8: Backward-facing step, high Reynolds number. (a) Mean velocity; (b) streamwise turbulence intensity; (c) Reynolds shear stress. □ Experimental data (Adams *et al.* 1984), ——— TLM-Algebraic, — — — TLM-SA.

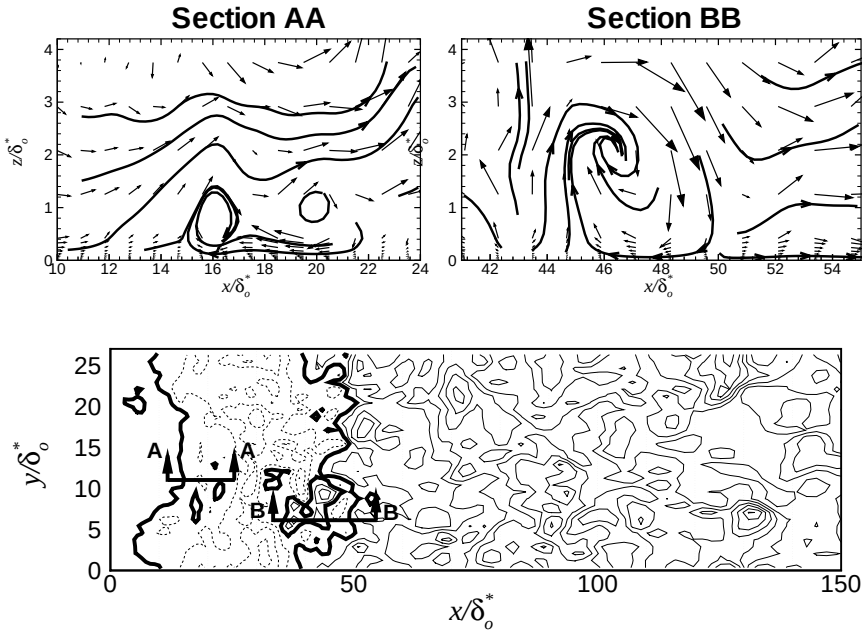

Figure 8.9: Contours of the instantaneous wall stress (bottom) and velocity vectors and streamlines in the $x - z$ plane (top). Low Reynolds number case.

8.4 Conclusions

In the present study the TLM coupled with a more sophisticated turbulence model was tested. Computations of the flow over a backward-facing step where performed at two Reynolds numbers. In general the main features of the flow field were captured accurately despite the limited resolution implied by the use of approximate wall boundary conditions.

More specifically, the reattachment point was predicted very accurately in both cases and was within 2% of the reference data. In addition the secondary bubble that is present at the step corner was also captured well, and had similar shape and size as in the reference data. The TLM coupled with the Spalart-Allmaras (1994) model also gave fairly accurate prediction of the skin friction coefficient. The mean velocity profiles and turbulent statistics were also in good agreement with the reference DNS end experimental data. The influence of the wall-model is limited to the first grid point off the wall. The coupling between the inner and outer layer computations, as shown by the examination of the mean and instantaneous velocity fields is satisfactory, indicating that the set of boundary conditions for the velocity and viscosity is appropriate.

Compared with the TLM coupled with a simple mixing length model the present version appears to be more accurate. This is particularly clear in the predicted skin friction coefficient. When the mixing-length model is used the flow, especially in the recirculating region, appears to be faster or slower depending in the Reynolds number. The rest of the turbulent statistics, however, are not influenced dramatically. This could be due to the fact that the wall model does not affect greatly the outer flow, which is dominated by the inviscid shear layer which is developing from the step edge. Proper resolution of this layer was found to be very important for the accuracy of the statistics.

The computational overhead of the model is of the order of 10%, compared with the standard formulation with the algebraic model, and appears cost-efficient. The accuracy of the approach, however, in flows with three-dimensional mean and flows where separation is caused by pressure gradients should be examined.

Acknowledgments

This work was supported by the Office of Naval Research under Grant No. N000149910960 monitored by Drs. L. Patrick Purtell and Candace Wark.

References

[1] ADAMS, E. W., JOHNSTON, J. P., AND EATON, J. K.(1984) *Report MD-43*, Department of Mechanical Engineering, Stanford University.

[2] AKSELVOLL, K., AND MOIN, P. (1995) *Report TF-63*, Department of Mechanical Engineering, Stanford University.

[3] BALARAS, E. AND BENOCCI, C. (1994) *AGARD CP 551*, 2.1–.

[4] BALARAS, E., BENOCCI, C., AND PIOMELLI, U. (1996) *AIAA J.* **34**, 1111–1119.

[5] BROOKE, J. W. AND HANRATTY, T. J. (1993) *Phys. Fluids A* **5**, 1011–1022.

[6] CABOT, W. (1995) *Annual Research Brief*, Center for Turbulence Research, Stanford University, 41–50.

[7] CABOT, W. AND MOIN, P. (1999) *Flow, Turbulence and Combustion* **63**, 269-291.

[8] CHAPMAN, D. (1979) *AIAA J.* **17**, 1293–1313.

[9] DEARDORFF, J. (1969) *J. Fluid Mech.* **41**, 453–480.

[10] JOHNSON, D. A. AND KING, L. S. (1985) *AIAA J.* **23**, 1684–1692.

[11] LE, H. AND MOIN, P. (1994) *Report TF-58*, Department of Mechanical Engineering, Stanford University.

[12] NIKITIN, N. V., NICOUD, F., WASISTHO, B., SQUIRES, K. D., AND SPALART, P. R. (2000) *Phys. Fluids* **12**, 1629–1632.

[13] PIOMELLI, U., FERZIGER, J. H., MOIN, P., AND KIM, J. (1989) *Phys. Fluids A* **1**, 1061–1068.

[14] PIOMELLI, U. AND LIU, J. (1995) *Phys. Fluids A* **7**, 839–848.

[15] SCHUMANN, U. (1974) *J. Comput. Phys.* **18**, 376–404.

[16] SPALART, P. R. AND ALLMARAS, S. R.(1994) *Rech. Aérospatiale* **1**, 5–21.

[17] WANG, M. (1999) *Annual Research Brief* Center for Turbulence Research, Stanford University, 355–364.